The following example illustrates how a cold-shot reactor is designed to maximize conversion while satisfying stability margins.

EXAMPLE 6.3 *Optimal Bypass Distribution in a Three-Bed, Cold-Shot, Ammonia Synthesis Converter*

A reactor for the synthesis of ammonia consists of three adiabatic beds, shown in Figure 6.4. As summarized in Table 6.1, the reactor feed consists of two sources, the first of which is a make-up feed stream of 20,000 kmol/hr at 25°C and 150 atmospheres containing mainly hydrogen and nitrogen in the stoichiometric molar ratio of 3:1. Since ammonia synthesis gas is produced from naphtha and air, it contains small concentrations of methane, from naphtha, and argon, from air. Both of these species reduce the partial pressures of the reagents, and thus affect the reaction rate. The second feed, which contains larger concentrations of the inert components, is a recycle stream of 40,000 kmol/hr at 25°C and 150 atmospheres consisting of unreacted synthesis gas, recovered after removing the ammonia product. The converter consists of three cylindrical, 2-m-diameter adiabatic beds, packed with catalyst for bed lengths of 1.5 m, 2 m, and 2.5 m, respectively. The reactor feed is split into three branches, with the first branch becoming the main feed entering the first bed after being preheated by the hot reactor effluent from the third bed. The second and third branches, with flow fractions ϕ_1 and ϕ_2, respectively, are controlled by adjusting valves V-1 and V-2, and provide cold-shot cooling at the first and second bed effluents, respectively. It is desired to optimize the allocation of the bypass fractions to maximize the conversion in the converter.

SOLUTION

Ammonia is synthesized in a reversible reaction, whose rate is correlated by the Tempkin equation (Tempkin and Pyzev, 1940), expressed in terms of the partial pressures, in atmospheres, of the reacting species:

$$R_a = 10^4 e^{-91{,}000/RT} [P_{N_2}]^{0.5} [P_{H_2}]^{1.5} - 1.3 \times 10^{10} e^{-140{,}000/RT} [P_{NH_3}] \qquad (6.32)$$

where R_a is the rate of nitrogen disappearance in kmol/m^3−s, T is the temperature in K, P_i are the partial pressures of the reacting species in atm, and the activation energies for the forward and reverse reactions are in kJ/kmol. The species partial pressures can be expressed in terms of the ammonia mole fraction, x_{NH_3}, and the original feed composition:

$$P_{H_2} = \frac{F_o x_{f,H_2} - 1.5\xi}{F_o - \xi} P,\ P_{N_2} = \frac{F_o x_{f,N_2} - 0.5\xi}{F_o - \xi} P \text{ and}$$
$$P_{NH_3} = \frac{F_o x_{f,NH_3} + \xi}{F_o - \xi} P = x_{NH_3} P \qquad (6.33)$$

where F_o is the total molar flow rate of the combined reactor feed, $\xi = F_o(x_{NH_3} - x_{f,NH_3})/(1 + x_{NH_3})$ is the molar conversion, P is the operating pressure, and $x_{f,i}$ is the feed mole fraction of species i. Consequently, the rate of reaction can be computed as a function of the temperature and x_{NH_3}, as shown in Figure 6.5a for an operating pressure of 150 atm. The ridge of maximum reaction rate in composition–temperature space defines an optimal decreasing temperature progression that is to be approximated by the appropriate design and operation of the converter.

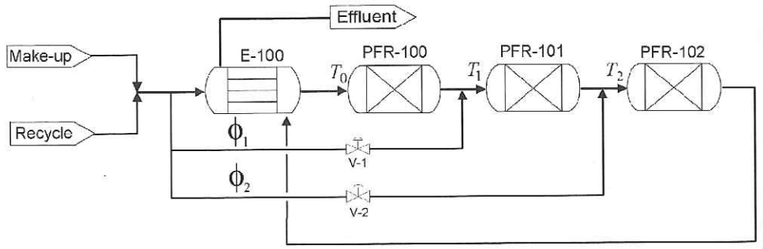

Figure 6.4 Cold-shot ammonia synthesis converter.

Table 6.1 Ammonia Converter—Make-up Feed and Recycle Streams

		Make-up stream	Recycle stream
Flow rate (kmol/hr)		20,000	40,000
Temperature (°C)		25	
Pressure (atm)		150	
Compositions (mol %):	H_2	72	61
	N_2	24	20
	NH_3	0	1.5
	CH_4	3	13
	Ar	1	4.5

The composition–temperature trajectory in the converter is plotted over contours of reaction rate in Figure 6.5b for suboptimal bypass fractions, $\underline{\phi} = [0.1, 0.1]^T$. Note that in the figure, the trajectories in the converter beds are solid lines, while those at the cold-shot mixing junctions are dotted lines. The temperature in Bed 1(PFR-100) rises to 415°C close to the equilibrium limit. The first cold shot cools the gas to 370°C. In Bed 2 (PFR-101), the temperature rises to 405°C, again close to the equilibrium limit. Before entering Bed 3, the final cold shot cools the gas to 360°C. The ammonia effluent concentration from the last bed is 12.7 mol%. Figure 6.5b also includes a dashed line for the optimal temperature progression when, instead of cold-shot cooling, heat is continuously removed while the reaction

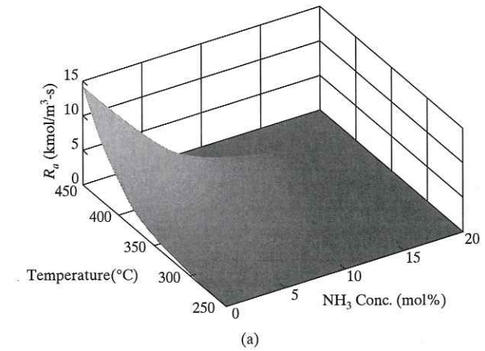

Figure 6.5 Composition–temperature space for ammonia synthesis converter: (a) reaction rate as a function of ammonia mole percent and temperature; (b) suboptimal cold-shot composition–temperature trajectory, plotted over reaction rate contours, with bypasses set to $\underline{\phi} = [0.1, 0.1]^T$.

proceeds in a single PFR. This line is the locus of maximum ammonia concentrations as a function of the reaction rate.

To maximize the conversion in the reactor, the following nonlinear program (NLP), of the type discussed in Chapter 18, is formulated:

$$\max_{\substack{\text{w.r.t.}\\ \phi_1,\,\phi_2}} \zeta \tag{6.34}$$

Subject to (s. t.)

$$f(x) = 0 \tag{6.35}$$

$$T_1 > 300°\text{C} \tag{6.36}$$

$$T_2 > 300°\text{C} \tag{6.37}$$

$$\phi_1 + \phi_2 \leq 0.6 \tag{6.38}$$

where Eq. (6.35) refers to the kinetics and material and energy balances for the converter in Figure 6.4, and Eqs. (6.36) and (6.37) define lower limits for the combined feed temperatures to the second and third beds. These minimum values are taken arbitrarily as 300°C, but are representative of minimum ignition temperatures. Note that in the first bed, where the rate of reaction, and with it the heat generation rate, is higher, the feed temperature is maintained constant at the lower value of 270°C, by appropriate design of the heat-exchanger, E-100. Finally, Eq. (6.38) ensures that a total maximum bypass of 60% is not exceeded, noting that this upper limit is arbitrary.

The NLP in Eqs. (6.34)–(6.38) is solved efficiently using successive quadratic programming (SQP), as described in Chapter 18. Figure 6.6a shows the optimal converged solution, which is obtained in four iterations. The final ammonia composition in the converter effluent is 15.9 mol%, obtained with optimal bypass fractions, $\phi_1 = 0.227$ and $\phi_2 = 0.240$. The composition–temperature trajectories for the optimal bypass distribution, shown in Figure 6.6b, confirm that the overall performance of the three beds is significantly improved through increased utilization of the second and third beds. These results can be reproduced with HYSYS.Plant, using the file NH3_CONVERTOR_OPT.hsc, and with ASPEN PLUS, using the file NH3_CONVERTOR.OPT.bkp. For full details, the reader is referred to the CD-ROM that accompanies this book, where this example is presented in multimedia tutorials under: *HYSYS → Tutorials → Reactor Design → Ammonia Converter Design*, and *ASPEN → Tutorials → Reactor Design Principles → Ammonia Converter Design*. Using simulators, complex reactor configurations are readily designed. ■

6.3 REACTOR NETWORK DESIGN USING THE ATTAINABLE REGION

This section describes the use of the attainable region (AR), which defines the achievable compositions that may be obtained from a network of chemical reactors. This is analogous to the topic of feasible product compositions in distillation, presented in Section 7.5. The attainable region in composition space was introduced by Horn (1964), with more recent developments and extensions by Glasser and co-workers (Glasser et al. 1987; Hildebrandt et al., 1990).

Figure 6.7 illustrates the attainable region for van de Vusse kinetics (van de Vusse, 1964), based on the reactions:

$$\text{A} \underset{k_2}{\overset{k_1}{\rightleftarrows}} \text{B} \xrightarrow{k_3} \text{C}$$

$$2\text{A} \xrightarrow{k_4} \text{D} \tag{6.39}$$

Reactions 1, 2, and 3 are first-order in A, B, and B, respectively, while reaction 4 is second-order in A. The rate constants at a particular temperature are: $k_1 = 0.01\ \text{s}^{-1}$, $k_2 = 5\ \text{s}^{-1}$, $k_3 = 10\ \text{s}^{-1}$, and $k_4 = 100\ \text{m}^3/\text{kmol}\cdot\text{s}^{-1}$. The boundary of the attainable region, shown in Figure 6.7, is composed of arcs, each of which results from the application of a distinct reactor type, as described next.

For the case of van de Vusse kinetics with a feed of 1 kmol/m^3 of A, Figure 6.7 indicates that the AR boundary is composed of an arc representing a CSTR with bypass (curve C), a

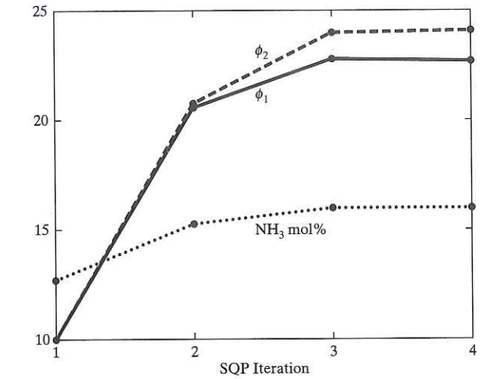

(a)

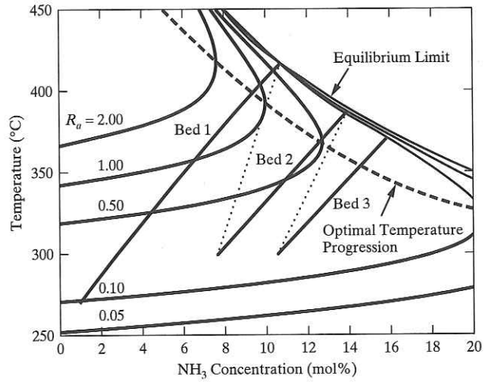

(b)

Figure 6.6 Optimal selection of bypass fractions for cold-shot ammonia converter: (a) convergence to the optimal solution; (b) optimal cold-shot profile in composition–temperature space with bypasses set to $\phi_2 = [0.227, 0.240]^T$.

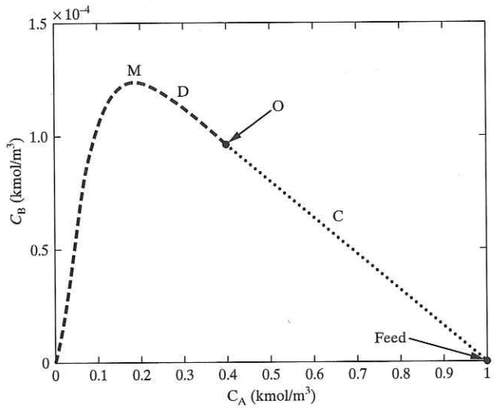

Figure 6.7 Attainable region for the van de Vusse reactions.

CSTR (point O), and a CSTR followed by a PFR (curve D). Within the region bounded by the three arcs and the horizontal base line ($C_B = 0$), product compositions can be achieved with some combination of these reactor configurations. The appropriate reactor configuration along the boundary of the attainable region depends on the desired effluent concentration of A. When $1 > C_A > 0.38$ kmol/m^3, a CSTR with bypass (curve C) provides the maximum concentration of B, while when $C_A < 0.38$ kmol/m^3, this is achieved using a CSTR (point O), followed by a PFR (Curve D). Note that the maximum achievable concentration, $C_B = 1.25 \times 10^{-4}$ kmol/m^3, is obtained using a CSTR followed by a PFR (at point M along curve D). Evidently, the attainable region provides helpful assistance in the design of optimal reactor networks. A procedure for the construction of attainable regions is discussed next.

Construction of the Attainable Region

A systematic method for the construction of the attainable region using CSTRs and PFRs, with or without mixing and bypass, for a system of chemical reactions, as presented by Hildebrandt and Biegler (1995), is demonstrated for van de Vusse kinetics:

Step 1: *Begin by constructing a trajectory for a PFR from the feed point, continuing to the complete conversion of A or chemical equilibrium.* In this case, the PFR trajectory is computed by solving simultaneously the kinetic equations for A and B:

$$\frac{dC_A}{d\tau} = -k_1 C_A + k_2 C_B - k_4 C_A^2 \tag{6.40}$$

$$\frac{dC_B}{d\tau} = k_1 C_A - k_2 C_B - k_3 C_B \tag{6.41}$$

where τ is the PFR residence time. Note that kinetic equations for C and D are not required for the construction of the attainable region in two-dimensional space because their compositions do not appear in Eqs. (6.40) and (6.41). The trajectory in $C_A - C_B$ space is plotted in Figure 6.8a as curve ABC. In this example, component A is completely converted.

Step 2: *When the PFR trajectory bounds a convex region, this constitutes a candidate attainable region. A convex region is one in which all straight lines drawn from one point on the boundary to any other point on the boundary lie wholly within the region or on the boundary. If not, the region is nonconvex. When the rate vectors, $[dC_A/d\tau, dC_B/d\tau]^T$ at concentrations outside of the candidate AR do not point back into it, the current limits are the boundary of the AR and the procedure terminates.* In this example, as seen in Figure 6.8a, the PFR trajectory is not convex from A to B, so proceed to the next step to determine if the attainable region can be extended beyond the curve ABC.

Step 3: *The PFR trajectory is expanded by linear arcs, representing mixing between the PFR effluent and the feed stream, extending the candidate attainable region. Note that a linear arc connecting two points on a composition trajectory is expressed by the equation:*

$$\underline{c}^* = \alpha \underline{c}_1 + (1 - \alpha)\underline{c}_2 \tag{6.42}$$

where $\underline{c}_1$ and $\underline{c}_2$ are vectors for two streams in the composition space, $\underline{c}^*$ is the composition of the mixed stream, and α is the fraction of the stream with composition $\underline{c}_1$ in the mixed stream. The linear arcs are then tested to ensure that no rate vectors positioned on them point out of the AR. If there are such vectors, proceed to the next step, or return to step 2. As shown in Figure 6.8a, a linear arc, ADB, is added, extending the attainable region to ADBC. Since for this example, rate vectors computed along this arc are found to point out of the extended AR, proceed to the next step.

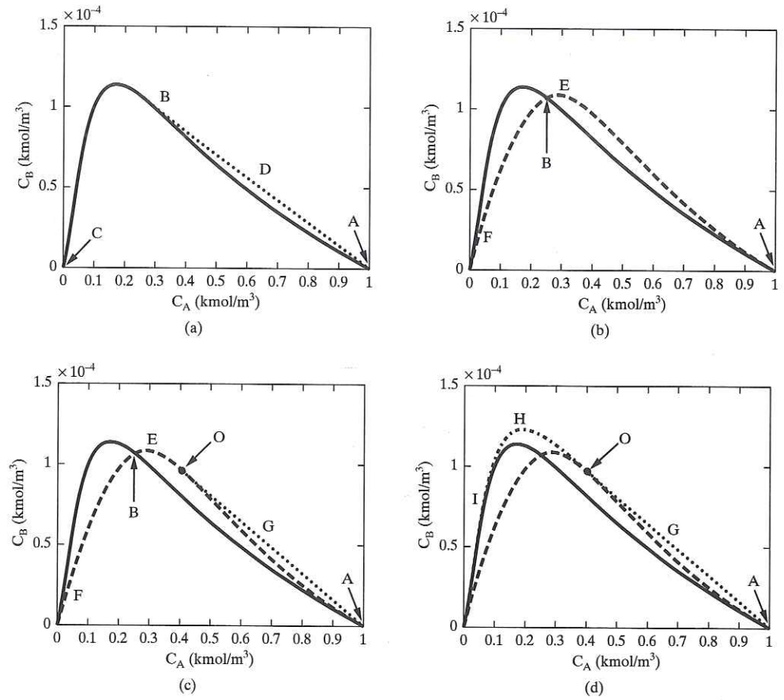

Figure 6.8 Construction of the attainable region for the van de Vusse reaction: (a) PFR trajectory from $\underline{C}(0) = [1, 0]^T$ (solid line), with mixing line (dotted line); (b) CSTR trajectory from $\underline{C}(0) = [1, 0]^T$ (dashed line); (c) addition of bypass to CSTR (dotted line); (d) addition of PFR in series with CSTR (dot-dashed line).

Step 4: *Since there are vectors pointing out of the convex hull, formed by the union between the PFR trajectory and linear mixing arcs, it is possible that a CSTR trajectory enlarges the attainable region. After placing the CSTR trajectory that extends the AR the most, additional linear arcs that represent the mixing of streams are placed to ensure that the AR remains convex.* The CSTR trajectory is computed by solving the CSTR form of the kinetic equations for A and B, given by Eqs. (6.40) and (6.41) as a function of the residence time, τ:

$$C_{A0} - C_A = \tau(k_1 C_A - k_2 C_B + k_4 C_A^2) \tag{6.43}$$

$$C_B = \tau(k_1 C_A - k_2 C_B - k_3 C_B) \tag{6.44}$$

For this example, the CSTR trajectory that extends the AR most is that computed from the feed point, at C_{A0}, the largest concentration of A. This is indicated as curve AEF in Figure 6.8b, which passes through point B. Since the union of the previous AR and the CSTR trajectory is not convex, a linear arc, AGO, is augmented as shown in Figure 6.8c. This arc represents a CSTR with a bypass stream.

Step 5: *A PFR trajectory is drawn from the position where the mixing line meets the CSTR trajectory. If this PFR trajectory is convex, it extends the previous AR to form an*

expanded candidate AR. Then return to Step 2. Otherwise, repeat the procedure from Step 3. As shown in Figure 6.8d, the PFR trajectory, OHI, leads to a convex attainable region. The boundaries of the region are: (a) the linear arc, AGO, which represents a CSTR with bypass stream; (b) the point O, which represents a CSTR; and (c) the arc OHI, which represents a CSTR followed by a PFR in series. It is noted that the maximum composition of B is obtained at point H, using a CSTR followed by a PFR.

Clearly, the optimal reactor design minimizes the annualized cost, computed to account for the capital and operating costs, and not simply the design that maximizes the yield or selectivity. Nonetheless, the maximum attainable region identifies the entire space of feasible concentrations. The following example shows how the attainable region is used to select the most appropriate reactor network to maximize the yield of a desired product where a number of competing reactions occur.

EXAMPLE 6.4 *Reaction Network Synthesis for the Manufacture of Maleic Anhydride*

Maleic anhydride, $C_4H_2O_3$, is manufactured by the oxidation of benzene with excess air over vanadium pentoxide catalyst (Westerlink and Westerterp, 1988). The following reactions occur:

$$\text{Reaction 1:} \quad C_6H_6 + \tfrac{9}{2}O_2 \rightarrow C_4H_2O_3 + 2CO_2 + 2H_2O \tag{6.45}$$

$$\text{Reaction 2:} \quad C_4H_2O_3 + 3O_2 \rightarrow 4CO_2 + H_2O \tag{6.46}$$

$$\text{Reaction 3:} \quad C_6H_6 + \tfrac{15}{2}O_2 \rightarrow 6CO_2 + 3H_2O \tag{6.47}$$

Since air is supplied in excess, the reaction kinetics are approximated using first-order rate laws:

$$\text{A} \xrightarrow{r_1} \text{P} \xrightarrow{r_2} \text{B}, \qquad \text{A} \xrightarrow{r_3} \text{C}$$

$$r_1 = k_1C_A,\ r_2 = k_2C_P, \text{ and } r_3 = k_3C_A \tag{6.48}$$

In the above, A is benzene, P is maleic anhydride (the desired product), and B and C are the undesired byproducts (H_2O and CO_2). The rate coefficients for Eqs. (6.48) are (in m^3/kg catalyst ·s)

$$\left.\begin{aligned} k_1 &= 4{,}280 \exp\,[-12{,}660/T(\text{K})] \\ k_2 &= 70{,}100 \exp\,[-15{,}000/T(\text{K})] \\ k_3 &= 26 \exp\,[-10{,}800/T(\text{K})] \end{aligned}\right\} \tag{6.49}$$

Given that the available feed stream contains benzene at a concentration of 10 mol/m^3, with a volumetric flow rate, υ_0, of 0.0025 m^3/s (the feed is largely air), a network of isothermal reactors is proposed to maximize the yield of maleic anhydride.

First, an appropriate reaction temperature is selected. Following Heuristic 7 in Chapter 5, Figure 6.9 shows the effect of temperature on the three rate coefficients, and indicates that in the range $366 < T < 850$ K, the rate coefficient, k_1, of the desired reaction to MA is larger than those of the competing reactions. An operating temperature at the upper end of this range is recommended, as the rate of reaction increases with temperature.

Since all of the reaction rate expressions involve only benzene and maleic anhydride, the system can be expressed in a two-dimensional composition space. For this system, the attainable region is straightforward to construct. This begins by tracing the composition space trajectory for a packed bed reactor (PBR), modeled as a PFR, which depends on the solution of the molar balances:

$$\upsilon_0 \frac{dC_A}{dW} = -k_1C_A - k_3C_A, \qquad C_A(0) = C_{A0} = 10 \text{ mol/m}^3 \tag{6.50}$$

$$\upsilon_0 \frac{dC_P}{dW} = k_1C_A - k_2C_P, \qquad C_P(0) = 0 \text{ mol/m}^3 \tag{6.51}$$

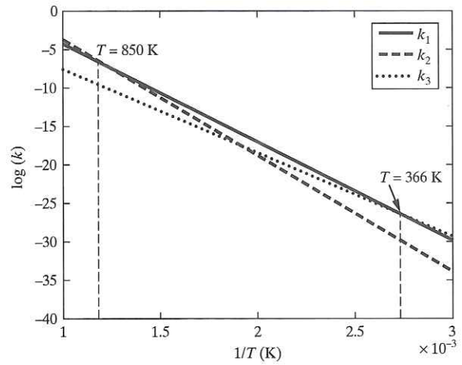

Figure 6.9 Influence of temperature on rate constants for MA manufacture.

where W is the kg of catalyst. In the above equations, the temperature-dependent rate constants are computed using Eqs. (6.49). Figure 6.10 presents solutions of these equations as trajectories in $C_A - C_P$ space for several operating temperatures. Since these trajectories are convex, and rate vectors computed along their boundaries are tangent to them, it is concluded that each trajectory bounds the attainable region for its corresponding temperature.

Evidently, a single plug-flow reactor (or packed-bed reactor in this case) provides the maximum production of maleic anhydride, with the required space velocity being that which brings the value of C_P to its maximum in Figure 6.10. At 800 K, it is determined that the maximum concentration of maleic anhydride is 3.8 mol/m^3, requiring 4.5 kg of catalyst. At 600 K it is 5.3 mol/m^3, but at this low temperature, 1,400 kg of catalyst is needed. A good compromise is to operate the PBR at an intermediate temperature, for example, 770 K, with a maximum concentration of maleic anhydride of 4.0 mol/m^3, requiring 8 kg of catalyst.

Figure 6.11a shows composition profiles for all species as a function of bed length (proportional to the weight of catalyst), indicating that the optimal catalyst loading, where the concentration of maleic anhydride is a maximum, is about 8 kg for isothermal operation at 770 K. Figure 6.11b indicates that the yield (the ratio of the desired product rate and feed rate) under these conditions is 61%, while the selectivity is only about 10%. The selectivity (the ratio of the desired product and total products) for this reaction system is poor, due to the large amounts of CO_2 and H_2O produced, with the highest selectivity, achieved by repressing both of the undesired reactions, at 22%. ■

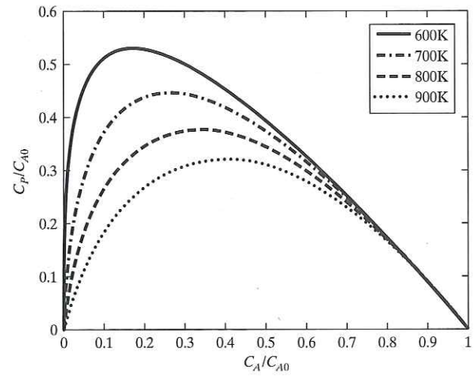

Figure 6.10 Attainable regions for MA manufacture at various temperatures.

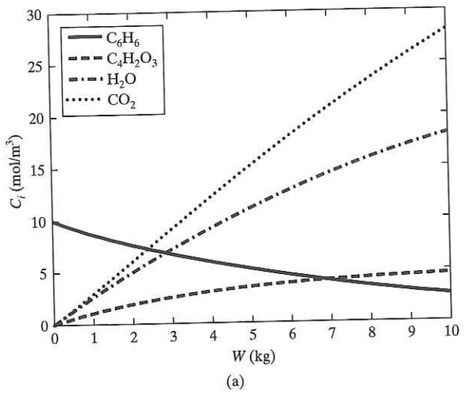

(a)

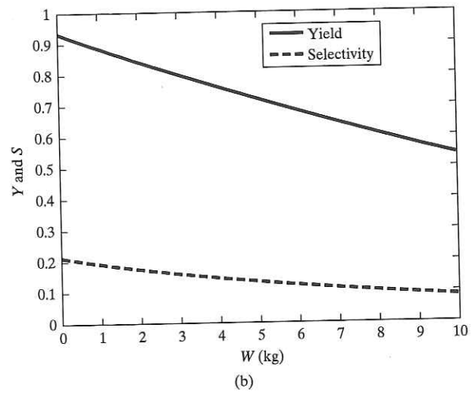

(b)

Figure 6.11 Composition profiles for MA manufacture in an isothermal PBR at 770 K: (a) composition profiles; (b) selectivity and yield.

Thus far, the attainable region has been shown for the analysis of systems with two key compositions to be tracked. In the following, the principle of reaction invariants is used to reduce the composition space in systems of larger dimension.

The Principle of Reaction Invariants

Because the attainable region depends on geometric constructions, it is effectively limited to the analysis of systems involving two independent species. However, as shown by Omtveit et al. (1994), systems involving higher dimensions can be analyzed using the two-dimensional AR approach by applying the principle of reaction invariants of Fjeld et al. (1974). The basic idea consists of imposing atom balances on the reacting species. These additional linear constraints impose a relationship between the reacting species, permitting the complete system to be projected onto a reduced space of independent species. The AR analysis above may be used when this reduced space is in two dimensions.

Let the reacting system consist of n_i moles of each species i, each containing a_{ij} atoms of element j. The molar changes in each of the species due to reaction are combined in the vector $\Delta\underline{n}$, and the coefficients a_{ij} form the atom matrix $\underline{\underline{A}}$, noting that since the number of gram-

atoms for each element remain constant, $\underline{\underline{A}}\,\Delta\underline{n} = 0$. Partitioning $\Delta\underline{n}$ and $\underline{\underline{A}}$ into dependent, d, and independent, i, components:

$$\underline{\underline{A}} = [\underline{\underline{A}}_d \mid \underline{\underline{A}}_i] \tag{6.52}$$

$$\Delta\underline{n}^T = [\Delta\underline{n}_d^T \mid \Delta\underline{n}_i^T] \tag{6.53}$$

Assuming that $\underline{\underline{A}}_d$ is square and nonsingular, an expression for the changes in the number of moles of each dependent species is obtained by algebraic manipulation:

$$\Delta\underline{n}_d = -\underline{\underline{A}}_d^{-1}\,\underline{\underline{A}}_i\Delta\underline{n}_i \tag{6.54}$$

The dimension of i is equal to the number of species minus the number of elements (atoms) in the species. When this dimension is two or less, the principle of reaction invariants permits the application of the attainable region to complex reaction systems. This is illustrated in the following example, introduced by Omtveit et al. (1994).

EXAMPLE 6.5 *Attainable Region for Steam Reforming of Methane*

Construct the attainable region for the steam reforming of methane at 1,050 K, and use it to identify the networks that provide for the maximum composition and selectivity of CO.

SOLUTION

The following reactions, involving five species and three elements, dominate in the steam reforming of methane:

$$CH_4 + 2H_2O \rightleftharpoons CO_2 + 4H_2 \tag{6.55}$$
$$CH_4 + H_2O \rightleftharpoons CO + 3H_2 \tag{6.56}$$
$$CO + H_2O \rightleftharpoons CO_2 + H_2 \tag{6.57}$$

By evoking the principle of reaction invariants, the number of species that need to be tracked for this system is reduced to two so that the attainable region can be shown in two dimensions. Accordingly, the vector of molar changes is

$$\Delta\underline{n}^T = [\Delta\underline{n}_d^T \mid \Delta\underline{n}_i^T] = [\Delta n_{H_2}, \Delta n_{H_2O}, \Delta n_{CO_2} \mid \Delta n_{CH_4}, \Delta n_{CO}]^T \tag{6.58}$$

where methane and carbon monoxide have been selected as the independent components. The atom balances for the three elements, C, H, and O, are

$$\begin{aligned} &\text{C balance:} && \Delta n_{CO_2} + \Delta n_{CH_4} + \Delta n_{CO} = 0 \\ &\text{H balance:} && 2\Delta n_{H_2} + 2\Delta n_{H_2O} + 4\Delta n_{CH_4} = 0 \\ &\text{O balance:} && \Delta n_{H_2O} + 2\Delta n_{CO_2} + \Delta n_{CO} = 0 \end{aligned}$$

The atom matrix $\underline{\underline{A}}$ with rows corresponding to C, H, and O, respectively, is

$$\underline{\underline{A}} = [\underline{\underline{A}}_d \mid \underline{\underline{A}}_i] = \left[\begin{array}{ccc|cc} 0 & 0 & 1 & 1 & 1 \\ 2 & 2 & 0 & 4 & 0 \\ 0 & 1 & 2 & 0 & 1 \end{array}\right] \tag{6.59}$$

The dependent molar changes, $\Delta\underline{n}_d$, are expressed in terms of the molar changes in methane and carbon monoxide, using Eq. (6.54):

$$\Delta\underline{n}_d = \begin{bmatrix} \Delta n_{H_2} \\ \Delta n_{H_2O} \\ \Delta n_{CO_2} \end{bmatrix} = -\underline{\underline{A}}_d^{-1}\,\underline{\underline{A}}_i\Delta\underline{n}_i = \begin{bmatrix} -4 & -1 \\ 2 & 1 \\ -1 & -1 \end{bmatrix}\begin{bmatrix} \Delta n_{CH_4} \\ \Delta n_{CO} \end{bmatrix} \tag{6.60}$$

For example, if $\Delta n_{CH_4} = -5$ mol and $\Delta n_{CO} = 3$ mol, Eq. (6.60) gives $\Delta n_{H_2} = 17$ mol, $\Delta n_{H_2O} = -7$ mol, and $\Delta n_{CO_2} = 2$ mol. The feed would have to contain more than 5 moles of methane and 7 moles of water.

Xu and Froment (1989) provide the kinetic expressions for the reversible reactions in Eqs. (6.55)–(6.57) in terms of the partial pressures of the participating species. Noting that the number of moles increases by two in each of the reactions in which methane is consumed, the total number of moles in the system is given by

$$n_T = [n_{H_2} + n_{H_2O} + n_{CO_2} + n_{CH_4} + n_{CO}]_0 - 2\Delta n_{CH_4} \tag{6.61}$$

The partial pressure of each of the five species is expressed as: $P\, n_i/n_T$, for i, where the number of moles of the dependent species, H_2, H_2O, and CO_2 are expressed in terms of the number of moles of CH_4 and CO using Eq. (6.60). This allows the construction of the attainable region for the steam reforming reactions at 1,050 K, which was computed by Omtveit et al. (1994) as follows:

Step 1: *Begin by constructing a trajectory for a PFR from the feed point, continuing to the complete conversion of methane or chemical equilibrium.* Here, the PFR trajectory is computed by solving the kinetic equations for the reactions of Eqs. (6.55)–(6.57) to give the mole numbers of CH_4 and CO. This leads to trajectory (1) in Figure 6.12, which tracks the compositions from the feed point, A, to chemical equilibrium at point B.

Step 2: *When the PFR trajectory bounds a convex region, this constitutes a candidate attainable region. When the rate vectors at concentrations outside of the candidate AR do not point back into it, the current limits are the boundary of the AR and the procedure terminates.* In Figure 6.12, the PFR trajectory is not convex, so proceed to the next step.

Step 3: *The PFR trajectory is expanded by linear arcs, representing mixing between the PFR effluent and the feed stream, extending the candidate attainable region.* Here, two linear arcs are introduced to form a convex hull, tangent to the PFR trajectory from below, connecting to the chemical equilibrium point B (line 2), and from the feed point to a point tangent to the PFR trajectory from above (line 3). In this example, line 2 constitutes the lower boundary of the attainable region. It is found that rate trajectories point out of the convex hull, so proceed to the next step.

Step 4: *Since there are vectors pointing out of the convex hull, formed by the union between the PFR trajectory and linear mixing arcs, a CSTR trajectory may enlarge the attainable region. After placing the CSTR trajectory that extends the AR the most, additional linear arcs that represent the mixing of streams are placed to ensure that the AR remains convex.* Here, the CSTR trajectory is computed by solving the molar balances for CH_4 and CO as the residence time, τ, varies. This gives trajectory (4), augmented by two linear arcs, connecting the feed point to a point tangent to the CSTR trajectory (line 5) at point C, and an additional line (6) connecting the CSTR to the PFR trajectories at two tangent points. This forms the new candidate attainable region, on which trajectories are identified that point outwards.

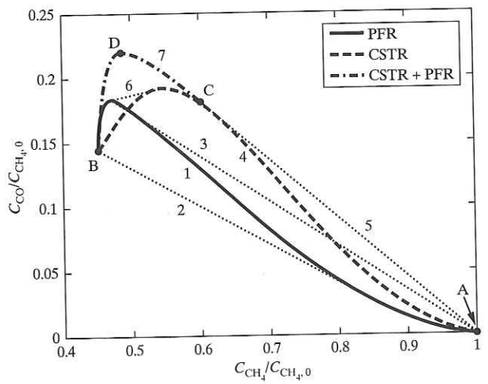

Figure 6.12 Development of the attainable region for steam-reforming reactions at $T = 1{,}050$ K.

Step 5: *A PFR trajectory is drawn from the position where the mixing line meets the CSTR trajectory. When this PFR trajectory is convex, it extends the previous AR to form an expanded candidate AR. Return to Step 2. Otherwise, repeat the procedure from Step 3.* As shown in Figure 6.12, the PFR trajectory (line 7) leads to a convex attainable region. The boundaries of the region are: (a) the linear arc (line 5) from A to C, which represents a CSTR with a bypass stream; (b) the point C, which represents a CSTR; and line 7 from C to B, which represents a CSTR followed by a PFR in series. Note that the maximum composition of CO is obtained at point D, using a CSTR and PFR in series. The maximum selectivity, defined by the ratio of CO/CH_4, is also achieved at point D, where the ratio is 0.47, as compared to point C, where the ratio is only 0.30. ■

6.4 SUMMARY

This chapter has introduced the design of chemical reactors and reactor networks. Different methods of reaction temperature control have been presented, with emphasis on the use of multiple adiabatic reactors or beds, using cold shots or heat exchangers between reactors or beds. The attainable region is presented to define the reactor network that maximizes either the yield or the selectivity of a desired product, given the feed to the reactor. However, since reactor yield is often sacrificed in favor of selectivity, conversion is rarely complete, with unreacted species recycled. Thus, the optimal reactor feed conditions depend on the plant economics and the reactor network should be synthesized as part of an overall plant design, as described in Chapter 8. In addition, the reader is referred to Biegler et al. (1997) and Floudas (1995), for mixed-integer nonlinear programming (MINLP) approaches, which address this plantwide process optimization. As seen in Examples 10.15 and 10.16, MINLP approaches begin by constructing a superstructure of possible design configurations, with the optimal design being a subset of the superstructure. Note that many modern MINLP approaches for the design of plants involving reactor networks draw on the AR method for superstructure construction.

After completing this chapter and reviewing the CD-ROM that accompanies this book, the reader should

1. be able to use effectively ASPEN PLUS and/or HYSYS.Plant to model chemical reactors, implementing complex configurations involving tube cooling and cold shots.
2. have an appreciation for the complex configurations that are often used in commercial reactor designs, especially when it is required to handle highly exothermic or endothermic reactions.
3. be able to define the combination of CSTRs and/or PFRs that maximize the yield or selectivity of the desired reactor product for a particular feed composition, given the reaction kinetics, using attainable region analysis.

REFERENCES

Aris, R., "The Optimum Design of Adiabatic Reactors with Several Beds," *Chem. Eng. Sci.*, **12**, 243 (1960).

Biegler, L.T., I.E. Grossmann, and A.W. Westerberg, *Systematic Methods of Chemical Process Design*, Prentice-Hall, Upper Saddle River, New Jersey (1997).

Felder, R.M., and R.W. Rousseau, *Elementary Principles of Chemical Processes*, Third Edition, John Wiley & Sons, New York, pp. 451–452 (2000).

Fjeld, M., O.A. Asbjornsen, and H.J. Astrom, "Reaction Invariants and their Importance in the Analysis of Eigenvectors, Stability and Controllability of CSTRs," *Chem. Eng. Sci.*, **30**, 1917 (1974).

Floudas, C.A., *Nonlinear and Mixed-integer Optimization: Fundamentals and Applications*, Oxford University Press, Oxford (1995).

Fogler, H.S., *Elements of Chemical Reaction Engineering*, Third Edition, Prentice-Hall, Englewood Cliffs, New Jersey (1999).

Glasser, D., C. Crowe, and D.A. Hildebrandt, "A Geometric Approach to Steady Flow Reactors: The Attainable Region and Optimization in Concentration Space," *Ind. Eng. Chem. Res.*, **26**(9), 1803 (1987).

Hildebrandt, D., and L.T. Biegler, "Synthesis of Chemical Reactor Networks", *AIChE Symp. Ser.* No. 304, Vol. 91, 52 (1995).

Hildebrandt, D.A., D. Glasser, and C. Crowe, "The Geometry of the Attainable Region Generated by Reaction and Mixing with and without Constraints," *Ind. Eng. Chem. Res.*, **29**(1), 49 (1990).

Horn, F.J.M., "Attainable Regions in Chemical Reaction Technique," in the *Third European Symposium of Chemical Reaction Engineering*, Pergamon Press, London (1964).

Levenspiel, O., *Chemical Reaction Engineering*, 3rd ed., Wiley, New York (1999).

Lewin, D.R., and R. Lavie, "Optimal Operation of a Tube Cooled Ammonia Converter in the Face of Catalyst Bed Deactivation," *I. Chem. Eng. Symp. Ser.*, **87**, 393 (1984).

Omtveit, T., J. Tanskanen, and K.M. Lien, "Graphical Targeting Procedures for Reactor Systems," *Comput.Chem. Eng.*, **18**(S), S113 (1994).

Rase, H.F., *Chemical Reactor Design for Process Plants, Volume Two: Case Studies and Design Data*, Wiley-Interscience, New York (1977).

Schmidt, L.D., *The Engineering of Chemical Reactions*, Oxford University Press, Oxford (1998).

Smith, J.M., *Chemical Engineering Kinetics*, 3rd ed., McGraw-Hill, New York (1981).

Stephens, A.D., and R.J. Richards, "Steady State and Dynamic Analysis of an Ammonia Synthesis Plant," *Automatica*, **9**, 65 (1973).

Temkin, M., and V. Pyzhev, "Kinetics of Ammonia Synthesis on Promoted Iron Catalyst," *Acta Physicochim. U.R.S.S.*, **12**(3), 327 (1940).

Trambouze, P.J., and E.L. Piret, "Continuous Stirred Tank Reactors: Designs for Maximum Conversions of Raw Materials to Desired Product," *AIChE J.*, **5**, 384 (1959).

van de Vusse, J. G., "Plug Flow vs. Tank Reactor," *Chem. Eng. Sci.*, **19**, 994 (1964).

van Heerden, C., "Autothermic Processes—Properties and Reactor Design," *Ind. Eng. Chem.*, **45**(6), 1242 (1953).

Westerlink, E.J., and K.R. Westerterp, "Safe Design of Cooled Tubular Reactors for Exothermic Multiple Reactions: Multiple Reaction Networks," *Chem. Eng. Sci.*, **43**(5), 1051 (1988).

Xu, J., and G. Froment, "Methane Steam Reforming: Diffusional Limitations and Reactor Simulation," *AIChE J.*, **35**(1), 88 (1989).

EXERCISES

6.1 Carry out a modified design for the ammonia converter in Example 6.3, consisting of three diabatic reactor bed sections, each of 2 m diameter and 2 m length (note that the total bed length is the same as before). Assuming the same reactor inlet temperature of 270°C, compute the optimal heat duties and effluent temperatures for each bed, such that the effluent ammonia mole fraction for the reactor is maximized. Plot the temperature composition trajectory for the modified converter design and compare it to the three-bed cold-shot design of Example 6.3.

6.2 A system of three parallel reactions (Trambouze and Piret, 1959) is:

$$A \xrightarrow{k_1} B \quad A \xrightarrow{k_2} C \quad A \xrightarrow{k_3} D$$

where the reactions are zero-order, first-order, and second-order, respectively, with $k_1 = 0.025$ mol/L-min, $k_2 = 0.2$ min^{-1}, and $k_3 = 0.4$ L/mol-min, and the initial concentration of $C_A = 1$ mol/L. Use the attainable region algorithm to find the reactor network that maximizes the selectivity of C from A.

6.3 Repeat Exercise 6.2, taking the first two reactions as first order, and the last as second order, with $k_1 = 0.02$ min^{-1}, $k_2 = 0.2$ min^{-1}, and $k_3 = 2.0$ L/mol-min, and the initial concentration of $C_A = 1$ mol/L. Use the attainable region method to find the reactor network that maximizes the selectivity of C from A.

6.4 For the reaction system:

$$\begin{array}{ccccc} A + B & \xrightarrow{r_1} & C + A & \xrightarrow{r_2} & E \\ & \searrow^{r_3} & & \nearrow_{r_4} & \\ & & D + A & & \end{array}$$

where $r_1 = k_1 C_A^2$, $r_2 = k_2 C_C$, $r_3 = k_3 C_A$, and $r_4 = k_4 C_A$. The rate constants are $k_1 = 3$ m^3/kmol-min, $k_2 = 10$ min^{-1}, $k_3 = 0.5$ min^{-1}, $k_4 = 1.5$ min^{-1}, and the feed concentration of A is 1 kmol/m^3. Use the attainable region method to find the reactor network that maximizes the selectivity of C from A.

6.5 In Example 6.5, choose methane and hydrogen as independent components. Derive relationships for the mole numbers of the remaining components in terms of methane and hydrogen.

Chapter 7

Synthesis of Separation Trains

7.0 OBJECTIVES

Most chemical processes are dominated by the need to separate multicomponent chemical mixtures. In general, a number of separation steps must be employed, where each step separates between two components of the feed to that step. During process design, separation methods must be selected and sequenced for these steps. This chapter discusses some of the techniques for the synthesis of separation trains. More detailed treatments are given by Douglas (1995), Barnicki and Siirola (1997), and Doherty and Malone (2001).

After studying this chapter, the reader should

1. Be familiar with the more widely used industrial separation methods and their basis for separation.
2. Understand the concept of the separation factor and be able to select appropriate separation methods for vapor, liquid, and solid–fluid mixtures.
3. Understand how distillation columns are sequenced and how to apply heuristics to narrow the search for a near-optimal sequence.
4. Be able to apply algorithmic methods to determine an optimal sequence of distillation-type separations.
5. Be familiar with the difficulties in and techniques for determining feasible sequences when azeotropes can form.
6. Be able to determine feasible separation systems for gas mixtures and solid–fluid systems.

7.1 INTRODUCTION

Almost all chemical processes require the separation of mixtures of chemical species (components). In Section 5.4, three flowsheets (Figures 5.7, 5.8, and 5.9) are shown for processes involving a reactor followed by a separation system. A more general flowsheet for a process involving one reactor system is shown in Figure 7.1, where separation systems are shown before as well as after the reactor section. A *feed separation system* may be required to purify the reactor feed(s) by removing catalyst poisons and inert species, especially if present as a significant percentage of the feed. An *effluent separation system*, which follows the reactor system and is almost always required, recovers unconverted reactants (in gas, liquid, and/or solid phases) for recycle to the reactor system and separates and purifies products and byproducts. Where separations are too difficult, purge streams are used to prevent buildup of certain species in recycle streams. Processes that do not involve a reactor system also utilize

PRODUCT AND PROCESS DESIGN PRINCIPLES

Synthesis, Analysis, and Evaluation

Second Edition

Warren D. Seider

Department of Chemical and Biomolecular Engineering
University of Pennsylvania

J. D. Seader

Department of Chemical and Fuels Engineering
University of Utah

Daniel R. Lewin

Department of Chemical Engineering
Technion—Israel Institute of Technology

WILEY

John Wiley and Sons, Inc.

Executive Editor *Bill Zobrist*
Acquisitions Editor *Wayne Anderson*
Marketing Manager *Katherine Hepburn*
Media Editor *Martin Batey*
Senior Production Editor *Valerie A. Vargas*
Senior Designer *Kevin Murphy*
Cover Designer *Carol Grobe*
Outside Production Services *Ingrao Associates*

This book was set in Times Roman by UG / GGS Information Services, Inc. and printed and bound by Hamilton Printing. The cover was printed by Phoenix Color.

This book is printed on acid-free paper.

Library of Congress Cataloging-in-Publication Data:

Seider, Warren D.
Product and process design principles: synthesis, analysis, and evaluation / by Warren D. Seider, J. D. Seader, Daniel R. Lewin. — 2nd ed.
p. cm.
Rev. ed. of: Process design principles. ©1999.
ISBN 978-0-471-21663-6 (acid-free paper)
ISBN 978-0-471-45247-8 (WIE)
1. Chemical Processes I. Seader, J. D. II. Lewin, Daniel R. III. Seider, Warren D. Process Design Principles. IV. Title.
TP155.7.S423 2003
660′.2812—dc21

2002192252

Printed in the United States of America

10 9 8 7 6 5

To the memory of my parents, to Diane, and to Benjamin, Deborah, Gabriel, and Joe

To the memory of my parents, to Sylvia, and to my children

To my parents, Harry and Rebeca Lewin, to Ruti, and to Noa and Yonatan

To the memory of Richard R. Hughes, a pioneer in computer-aided simulation and optimization, with whom two of the authors developed many concepts for carrying out and teaching process design.